A drifting impact oscillator with periodic impulsive loading: Application to percussive drilling

A. Depouhon[a,b], V. Denoël[a], E. Detournay[b,c,*]

[a] *Structural Engineering, ArGEnCo, Department of Applied Sciences, Université de Liège, Belgium*
[b] *Department of Civil Engineering, University of Minnesota, MN, USA*
[c] *CSIRO Earth Science and Resource Engineering, Australia*

Abstract

Percussive drilling is extensively used to drill hard rocks in the earth resource industry, where it performs best compared to other drilling technologies. In this paper, we propose a novel model of the process that consists of a drifting oscillator under impulsive loading coupled with a bilinear force/penetration interface law, together with a kinetic energy threshold for continuous bit penetration. Following the formulation of the model, we analyze its steady-state response and show that there exists a parallel between theoretical and experimental predictions, as both exhibit a maximum of the average penetration rate with respect to the vertical load on bit. In addition, existence of complex long-term dynamics with the coexistence of periodic solutions in certain parameter ranges is demonstrated.

Keywords: Percussive drilling, Periodic orbit, Drifting oscillator, Impact system, Piecewise-linear system, Hybrid system

1. Introduction

Many industrial processes rely on the impulsive loading of a first body in contact with a second one to achieve the penetration of the former in the latter. Among these, we find nail hammering [1, 2] or pile driving [3–5]. Another such process is down-the-hole percussive drilling, where penetration is achieved by repeated application of a large impulsive force to a rock drill bit [6–8]. The impulsive force is generated by the impact of a pneumatically-operated piston (hammer) on a shank adapter (anvil). The kinetic energy conveyed by the piston is transformed into compressive stress waves upon contact with the adapter, waves that propagate through the drill bit down to the rock, leading to rock destruction by indentation, crushing and chipping [9].

Several authors have addressed the issue of modeling this process and have contributed to various aspects of the problem. Two foci of interest can be identified in the literature: (i) the bit/rock interaction, i.e. the interface law that captures the force/penetration behavior, and (ii) the bit dynamics, that is, the prediction of bit motion under specific loading and interface conditions. While the former topic has been addressed experimentally [10–13] and numerically based on a continuum approach [14, 15] or a discrete one [16], the study of bit dynamics has led to design considerations to maximize the process efficiency [9, 17], the development of numerical algorithms to simulate the process [7, 18], as well as the representation of the process as a drifting oscillator [19–21].

The phenomena taking place at the bit/rock interface are of very complex nature as several failure mechanisms result from the dynamic indentation of rock in the presence of debris remaining from former impacts. While some

*Corresponding author at: Department of Civil Engineering, University of Minnesota, MN, USA.
Email address: detou001@umn.edu (E. Detournay)

authors have proposed physics-based arguments to the development of interaction laws, based notably on the cavity expansion model [22], scaling arguments [23] or numerical evidence [14, 16], percussion drilling experiments have highlighted two common trends: (i) the force/penetration law consists of two successive phases, one associated with the loading and the other with the unloading of the interface [9, 11, 13, 24], and (ii) this law is rate-independent, i.e. it does not depend on the penetration velocity of the indenter [10, 24]. Furthermore, the idealization of this law by a history-dependent bilinear model, i.e. a linear spring with larger unloading stiffness than loading one, has been shown to capture the essential response observed in single impact indentation experiments as confirmed by measurements [13] and by the matching of numerical results to experimental ones in the analysis of stress waves traveling in drill steels [25].

Percussive drilling systems are known to exhibit an optimal functioning configuration, in the sense that a proper choice of the control parameters maximizes the bit average rate of penetration in the rock medium, as was evidenced from field measurements by [26] and conceptually presented in [27]. Works on bit dynamics have recovered this trend by modeling the drill bit as a drifting impact oscillator. In these models, a superposition of harmonic and static loadings was considered, at first, in combination with unilateral viscoelastic or perfectly rigid contact models serially connected to a constant-force threshold slider [19–21, 28] and, more recently, in combination with an interface law based on the elasto-plastic response of a rigid indenter in a semi-infinite medium [29]. Due to the unilateral nature of the contact, these models are non-smooth dynamical systems and belong to the class of piecewise-smooth systems; see the monograph by di Bernardo et al. [30] as well as the works by Leine et al. [31, 32] for an introduction to this category of systems.

In this paper, we introduce a model for the bit dynamics that also belongs to the family of drifting oscillators but differs in two key aspects from those proposed in [19–21, 28]. First, we consider the variable load on bit to be periodic impulsive rather than harmonic, a specificity that we presume more appropriate to model the activation related to repeated hammer blows. Second, we model the force/penetration behavior at the bit/rock interface by a modified bilinear law, partly tying up with the proposition of Ajibose [24, 29] to model the bit/rock interaction using power laws for the loading and unloading phases. A particularity of this second element is the introduction in the bit/rock interaction law of a kinetic energy barrier to dissociate static loadings from dynamic ones.

As we detail next, the model is deliberately kept as simple as possible in order to highlight the richness brought by these two features. Given the impulsive nature of the loading, the evolution of bit motion is ruled by continuous and discrete dynamics. As such, the proposed model belongs to the class of hybrid systems [30] that comprises, among others, models with impacting bodies, e.g. vibro-impact oscillators [33] or particle avalanche models [34].

Section 2 is the object of a detailed description of the model, with the introduction of its building blocks and governing equations. In Section 3, we present the results of the model analysis; in particular, we focus on its steady-state and long-term response. The paper then concludes with a discussion of the results in Section 4.

2. Mathematical modeling

The model is a 1 degree-of-freedom drifting oscillator subject to a combination of periodic impulsive and static loadings with a bilinear interface law coupled to a kinetic energy barrier describing the force/penetration characteristics. This formulation relies on several assumptions: (i) the existence of a timescale separation between the percussive activation on the one hand, and the bit motion as well as the bit/rock interaction on the other hand, allowing us to ignore wave propagation in the modeling of percussive drilling; (ii) the modeling of the bit/rock interaction

by a bilinear law that is essentially rate-independent, except for the existence of a kinetic energy threshold for the bit penetration; (iii) the reduction of the bit dynamics to the axial motion; and (iv) the neglect of debris cleaning. Despite these strong simplifying assumptions, this model captures the essence of the process response, and we believe it could be a proper springboard for the development of future more refined models of the process.

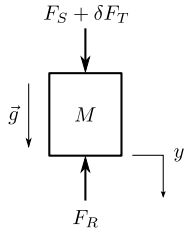

Figure 1: Free body diagram of the drill bit.

2.1. Governing equations

The bit free body diagram is shown in Figure 1. We denote the oscillator mass by M. Its vertical displacement y is positively defined in the downward direction. We refer to the static force and impulsive loading by F_S and δF_T, while the bit/rock interaction force is named F_R. The action of gravity is considered. The equation governing the bit dynamics is obtained by application of Newton's law

$$M\ddot{y} = Mg + F_S + \delta F_T - F_R. \tag{1}$$

The impulsive loading δF_T, resulting from the percussive activation, chosen to be of period T and of constant impulse I at each pulse, reads

$$\delta F_T(t) = I \sum_{i\in\mathbb{N}} \delta(t - iT - t_s), \tag{2}$$

with $\delta(\cdot)$ Dirac's delta function and $0 \leq t_s < T$ an arbitrary time shift. It is thus zero everywhere but at specific time instants spaced by a duration T, at which it increases the momentum of the bit. The equation of motion thus reduces to

$$M\ddot{y} = Mg + F_S - F_R, \tag{3}$$

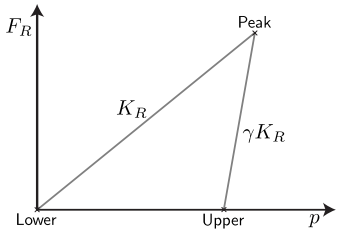

Figure 2: Bilinear bit/rock interaction law.

everywhere but at the instants of impact, $t_i = iT + t_s$, at which the bit velocity experiences an instantaneous jump

$$\dot{y}(t_i^+) = \dot{y}(t_i^-) + \frac{\eta I}{M}, \quad i \in \mathbb{N}, \tag{4}$$

where $0 \leq \eta \leq 1$ is an efficiency coefficient that accounts for the momentum transfer to the rock if the bit is in contact with the rock at the time of impact. This momentum transfer, which involves generation and propagation of waves in the rock medium, is assumed to take place instantaneously when viewed at the timescale of the bit motion; it can therefore be embodied in the coefficient η. For this preliminary study, however, we assume that $\eta = 1$, whether the bit is contacting the rock or not at the moment of application of the impulsive load. This approximation is in accordance with numerical simulations indicating that the maximum amount of dissipated energy is at most 5% of the impact energy of the piston when the bit is in contact with the rock [35].

2.2. Bit/rock interaction law

The rate-independent bilinear bit/rock interaction law, which relates the force on bit, F_R, to the penetration while drilling, p, follows from single impact dynamic indentation experiments. This law depends on two parameters: the loading stiffness K_R and the unloading one $\gamma K_R > K_R$. Figure 2 illustrates this relation and indicates along the drilling cycle three non-smooth locations with respect to the interaction law: the points of lower, peak and upper penetration. While penetration and bit position are equivalent in the frame of single impact experiments, this is no longer the case when considering repeated impacts. To

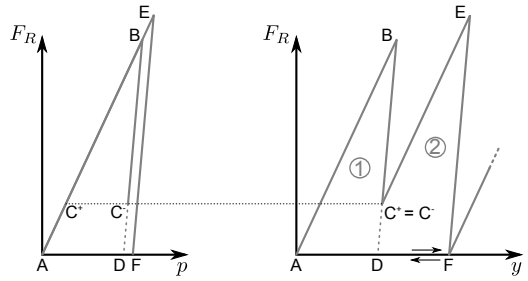

Figure 3: Bit/rock interaction model with force as a function of the bit penetration (left) and bit displacement (right).

relate the force on bit to the bit position, we define the penetration while drilling during the n^{th} drilling cycle as the advance of the bit with respect to the final contact position of the bit/rock interface during the previous drilling cycle plus the residual penetration, has the cycle not been completed

$$p^{(n)}(t) = y(t) - y_\ell^{(n)} + \frac{F_{R,\ell}^{(n)}}{K_R}. \tag{5}$$

Specific to this definition is the introduction of the history variables $y_\ell^{(n)}$ and $F_{R,\ell}^{(n)}$. These are defined as the bit position and the force on bit at the beginning of the n^{th} drilling cycle, the lower point of this cycle, hence index $_\ell$. Correspondences with the peak and upper drilling cycle locations, $(y_p^{(n)}, F_{R,p})$ and $(y_u^{(n)}, F_{R,u})$, can also be established when representing the bit/rock interaction law in the (y, F_R)-space. Figure 3 illustrates this match for two consecutive drilling cycles. Points A, C and F define the lower characteristics of drilling cycles while B and E are located at their peaks. The upper locations are denoted by D and F.

It is important to note that history variables do depend on the past trajectory of the system in a discrete manner. They capture the state of the bit/rock interaction law at a specific instant and, as such, evolve in a stepwise manner. Their update takes place at the instant the system goes through the corresponding non-smooth point of the interface law.

Following the definition of the penetration while drilling and those of the history variables, the bit/rock interaction law, in terms of the axial position, reads

$$F_R^{(n)}(y) = \begin{cases} F_{R,\ell}^{(n)} + K_R\left[y(t) - y_\ell^{(n)}\right] & \text{if loading,} \\ F_{R,p}^{(n)} + \gamma K_R\left[y(t) - y_p^{(n)}\right] & \text{if unloading,} \\ 0 & \text{if no contact.} \end{cases} \tag{6}$$

While experimental results do support the assumption of rate-independence embedded in the above interaction law, this independence must nonetheless be bounded above and below. The upper bound reflects the limit at which the indentation velocity cannot be neglected compared to the wave speed in the rock medium. The lower bound needs to be considered to account for cases when the bit is close to be at rest, to differentiate static and dynamic loadings. The upper bound is, in practice, never encountered but the lower one is and requires an adjustment of the interaction law. In that perspective, we complement the bilinear law with an energy barrier; that is, a new drilling cycle can only start provided the bit kinetic energy is larger than a given energy threshold E_ℓ^k

$$\frac{1}{2}M\dot{y}_\ell^2 \geq E_\ell^k. \tag{7}$$

This barrier dissociates the static indentation of rock from the dynamic one and is instantaneous at the timescale of bit motion. It implies that continuous penetration, i.e. over more than one drilling cycle, can only take place if the bit kinetic energy is larger than a threshold. This barrier leads to a direct loss of kinetic energy of the bit when a new drilling cycle is started. Equations (6) are thus complemented by the velocity update

$$\dot{y}_\ell^+ = \begin{cases} \sqrt{\dot{y}_\ell^{-2} - 2\frac{E_\ell^k}{M}} & \text{if } \dot{y}_\ell^- \geq \sqrt{2E_\ell^k/M}, \\ 0 & \text{otherwise,} \end{cases} \tag{8}$$

which drives the bit to a standstill should its kinetic energy be below the barrier. The symbols $\dot{y}_\ell^-$ and $\dot{y}_\ell^+$ refer to the velocities just before and after the beginning of the drilling cycle.

2.3. Drilling Phases

The conditional, in fact sequential, nature of the contact model conducts us to define four drilling phases.

(i) *Forward Contact* (FC): the bit motion is downwards while there is contact between the bit and the rock.

(ii) *Backward Contact* (BC): contact is established but the bit is moving upwards.

(iii) *Free Flight* (FF): the bit is flying off the hole bottom; the force exerted by the rock is zero.

(iv) *Standstill* (SS): the bit is at rest and in contact with the rock; the reaction force from the rock exactly compensates the vertical force on the bit.

With each regime, we then associate a specific expression of the equation of motion that we write in terms of the penetration while drilling rather than the bit position, given that $\dot{p}(t) = \dot{y}(t)$. Dropping the drilling cycle number for legibility, they read

$$\begin{aligned} \mathsf{FC}\ &: \quad M\ddot{p} + K_R p = Mg + F_S, \\ \mathsf{BC}\ &: \quad M\ddot{p} + \gamma K_R p = Mg + F_S + (\gamma - 1) K_R p_p, \\ \mathsf{FF}\ &: \quad M\ddot{p} = Mg + F_S, \\ \mathsf{SS}\ &: \quad \ddot{p} = \dot{p} = 0. \end{aligned} \tag{9}$$

They are completed by the velocity jump conditions of equations (4) and (8) where we set $\dot{y}(t) = \dot{p}(t)$ and $\eta = 1$. It is worth mentioning that our choice of representing the bit motion by the penetration while drilling rather than the position aims at preventing the drift of the system in the phase plane and ensures the boundedness of the state-space when studying the motion of the bit.

To complete the definition of the system dynamics, we introduce the conditions that govern the transition from one drilling phase to the other. Ten cases have to be considered. References to points in Figure 3 are made to illustrate their occurrence on the force/displacement response curve of the interface model.

- FC $\rightarrow$ BC: The drilling cycle reaches its peak, i.e. the bit velocity becomes zero, $\dot{p} = 0$; see points B and E.
- BC $\rightarrow$ FF: The drilling cycle completes at its upper point, i.e. the force on bit vanishes, $p = p_p\,(\gamma - 1)/\gamma$; point F represents this transition.
- FF $\rightarrow$ FC: A new drilling cycle begins, i.e. the bit reconnects with the hole bottom after a period of free flight, $p = p_u$, and has sufficient energy $\dot{p}_\ell \geq \sqrt{2E_\ell^k/M}$. This occurs at point F, where the penetration is reset to zero at the beginning of the next drilling cycle, $p_\ell = 0$.
- BC $\rightarrow \Delta\theta_i' \rightarrow$ FC: A new drilling cycle begins due to the percussive activation, i.e. the bit velocity changes sign before the current drilling cycle has completed, $\dot{p}_i^+ \cdot \dot{p}_i^- < 0$, and the activation increases the bit energy above the barrier; with this transition, a residual penetration exists at the beginning of the next drilling cycle, and $(p_\ell, F_{R,\ell}) > 0$. This corresponds to point C.

In case the energy of the bit is insufficient at the beginning of a drilling cycle, i.e. at a transition to forward contact, the bit motion is switched to standstill, in accordance with equation (8), and remains in that phase until the next activation takes place. Three transitions are thus possible: FF $\rightarrow$ SS, BC $\rightarrow$ SS and SS $\rightarrow \Delta\theta_i' \rightarrow$ FC. The transitions due to activation that do not lead to a change of drilling phase then complete the list: FC $\rightarrow \Delta\theta_i' \rightarrow$ FC, BC $\rightarrow \Delta\theta_i' \rightarrow$ BC and FF $\rightarrow \Delta\theta_i' \rightarrow$ FF.

2.4. Dimensionless formulation

For the ensuing analysis, it is convenient to reformulate the governing equations in dimensionless form. Choosing the timescale proportional to the resonant period of the spring/mass system associated with the bit/rock interface at loading, and the reference length scale as the peak penetration engendered by the only action of an activation on a bit at rest and in contact with the rock in the absence of energy barrier

$$t_* = \sqrt{\frac{M}{K_R}} \qquad \text{and} \qquad \ell_* = \frac{I}{\sqrt{MK_R}}, \tag{10}$$

we define the dimensionless time and penetration while drilling

$$\tau = \frac{t}{t_*} \qquad \text{and} \qquad \theta = \frac{p}{\ell_*}. \tag{11}$$

Inserting these in the governing equations, we obtain

$$\begin{aligned} \mathsf{FC}: &\quad \theta'' + \theta = \lambda_S, \\ \mathsf{BC}: &\quad \theta'' + \gamma\theta = \lambda_S + (\gamma - 1)\,\theta_p, \\ \mathsf{FF}: &\quad \theta'' = \lambda_S, \\ \mathsf{SS}: &\quad \theta'' = \theta' = 0, \end{aligned} \tag{12}$$

with $\lambda_S = (Mg + F_S)t_*/I$ the scaled total vertical dead load and θ_p the peak dimensionless penetration. Differentiation with respect to the dimensionless time is denoted by a prime symbol. The velocity jump $\Delta\theta_i' = \theta_i'^{+} - \theta_i'^{-}$ at impact times τ_i is equal to 1 and the impact times are given by

$$\tau_i = \tau - i\psi - \tau_s, \quad i \in \mathbb{N}_0, \tag{13}$$

where

$$\psi = \frac{T}{t_*}, \quad \tau_s = \frac{t_s}{t_*}.$$

The dimensionless transition conditions are obtained by replacing the dimensional penetration while drilling by its scaled counterpart in their expressions

$$\begin{aligned} &\mathsf{FC} \to \mathsf{BC}: \theta'(\tau) = 0, \\ &\mathsf{BC} \to \mathsf{FF}: \theta(\tau) = \frac{\gamma - 1}{\gamma}\theta_p, \\ &\mathsf{FF} \to \mathsf{FC}: \begin{cases} \theta(\tau) = \theta_u, \\ \theta'(\tau) \geq \kappa_0, \end{cases} \\ &\mathsf{FF} \to \mathsf{SS}: \begin{cases} \theta(\tau) = \theta_u, \\ \theta'(\tau) < \kappa_0, \end{cases} \\ &\mathsf{BC} \to \Delta\theta_i' \to \mathsf{SS}: \begin{cases} \theta_i'^{+} \cdot \theta_i'^{-} < 0, \\ \theta_i'^{+} < \kappa_0, \end{cases} \\ &\mathsf{BC} \to \Delta\theta_i' \to \mathsf{FC}: \begin{cases} \theta_i'^{+} \cdot \theta_i'^{-} < 0, \\ \theta_i'^{+} \geq \kappa_0, \end{cases} \\ &\mathsf{SS} \to \Delta\theta_i' \to \mathsf{FC}: \begin{cases} \tau = \tau_i, \\ \kappa_0 < 1, \end{cases} \\ &\mathsf{XX} \to \Delta\theta_i' \to \mathsf{XX}: \tau = \tau_i \end{aligned} \tag{14}$$

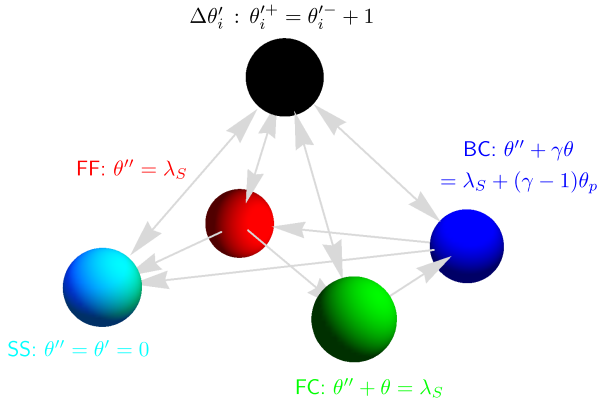

Figure 4: Sequential nature of the governing equations and authorized mode switches.

where $\kappa_0 = \sqrt{2E_\ell^k M}/I$ and $\mathsf{XX} \in \{\mathsf{FC}, \mathsf{BC}, \mathsf{FF}\}$.

While Table 1 provides typical orders of magnitude for the dimensionless parameters, Figure 4 illustrates the sequential nature of the system by showing the possible transitions between the modes; these are represented by gray arrows. Transitions within the base of the pyramid are state-dependent, e.g. $\mathsf{FC} \to \mathsf{BC}$, whereas those requiring percussive activation are time-related and transit through the apex of the pyramid, e.g. $\mathsf{SS} \to \Delta\theta_i' \to \mathsf{FC}$.

Parameter	γ	λ_S	$\Delta\theta_i'$	ψ	κ_0
Range	$(1, \infty)$	$[0.01, 1]$	1	$[10, 100]$	$[0, 1)$

Table 1: Typical ranges of the system parameters.

3. Limit-cycling behavior

Field and lab results have revealed the existence of an optimal control configuration of percussive drilling systems. In particular, these results have evidenced the existence of a feed force, i.e. the vertical load on bit, maximizing the average steady-state penetration rate [26, 27], as depicted in Figure 5. Our analysis therefore concentrates on the characterization of the steady-state response of the presented model and the identification of such a maximum for a given parametric configuration.

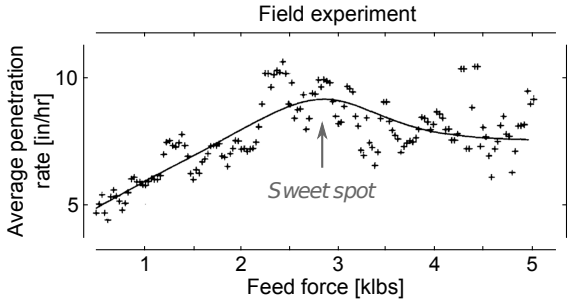

Figure 5: Existence of an optimal drilling configuration – Feed force influence on drilling performance. Experimental results from field measurements at Little Stobie Mine, Ontario, Canada. Adapted from Amjad [26].

3.1. Steady-state response computation

Given the hybrid nature of the governing equations, their time integration requires the implementation of a specific procedure. In the present case, we resort to a semi-analytical event-driven integration scheme. It consists of the standard three-stage strategy described by Acary and Brogliato [36]: (i) integrate the smooth vector field up to the next non-smooth event, (ii) accurately locate the time of this transition, and (iii) identify the next drilling phase and accordingly reinitialize the system at the event time. While stages (i) and (ii) are commonly performed numerically, we prefer to exploit the linear nature of the governing equations and the existence of a closed-form solution for the parametric equations of the trajectory, enabling these stages to be carried out analytically.

The computation of the steady-state response is performed via a shooting procedure [37, 38] enforcing a periodicity condition on the system trajectory in the phase plane. The convergence of this iterative procedure is contingent on two conditions: (i) the existence of a periodic response for the chosen limit cycle period, an integer multiple of the activation period since the system is non-autonomous [31], and (ii) the choice of a proper initial guess. Knowledge of the steady-state response directly yields that of the corresponding average penetration rate

$$v = \frac{1}{n\psi}\int_0^{n\psi} \theta'(s)\, ds = \frac{1}{n\psi}\sum_{m=1}^{M} \theta(\tau_m^-) - \theta(\tau_{m-1}^+), \quad (15)$$

with $n\psi$ the period of the limit cycle and the τ_m's denoting the times at which the $M-1$ phase transitions occur, $\tau_0 = 0$ and $\tau_M = n\psi$. In the sequel, we refer to variable n as the period multiplicity, i.e. the ratio of the limit cycle period to the excitation or fundamental period.

To assess the influence of the system parameters $(\gamma,\lambda_S,\psi,\kappa_0)$ on the average steady-state penetration rate, the shooting procedure has been embedded in an arclength-parameterized continuation one [37–39]. This predictor/corrector-based procedure allows the computation of solution branches upon variation of one parameter of the governing equations.

The determination of the stability of the limit cycles obtained via the shooting procedure is performed by computing the Floquet multipliers from the numerically evaluated monodromy matrix using finite differences [31, 38]. Specific care has been taken to handle the non-smooth and hybrid nature of the limit cycle by defining its origin at the peak location, a point that belongs to any limit cycle and at which the fundamental solution matrix is continuous. Also, a consistent initialization of the history variables was used to ensure the non-violation of the causality embedded in these variables. This procedure has been validated by analytical developments involving the calculation of saltation matrices at the discontinuity or non-smoothness points of the vector field, as detailed in [30, 31, 40]. Further details about the stability assessment procedure can be found in [41].

3.2. Characterization of periodic solutions

Periodic solutions, or limit cycles, can be characterized in several ways. To illustrate different descriptors, we consider two limit cycles that correspond to configuration $(\gamma,\lambda_S,\psi) = (10, 0.1, 15)$ with period multiplicity $n = 1$, and $\kappa_0 = 0.09$ (Figure 6) or $\kappa_0 = 0.24$ (Figure 7). These

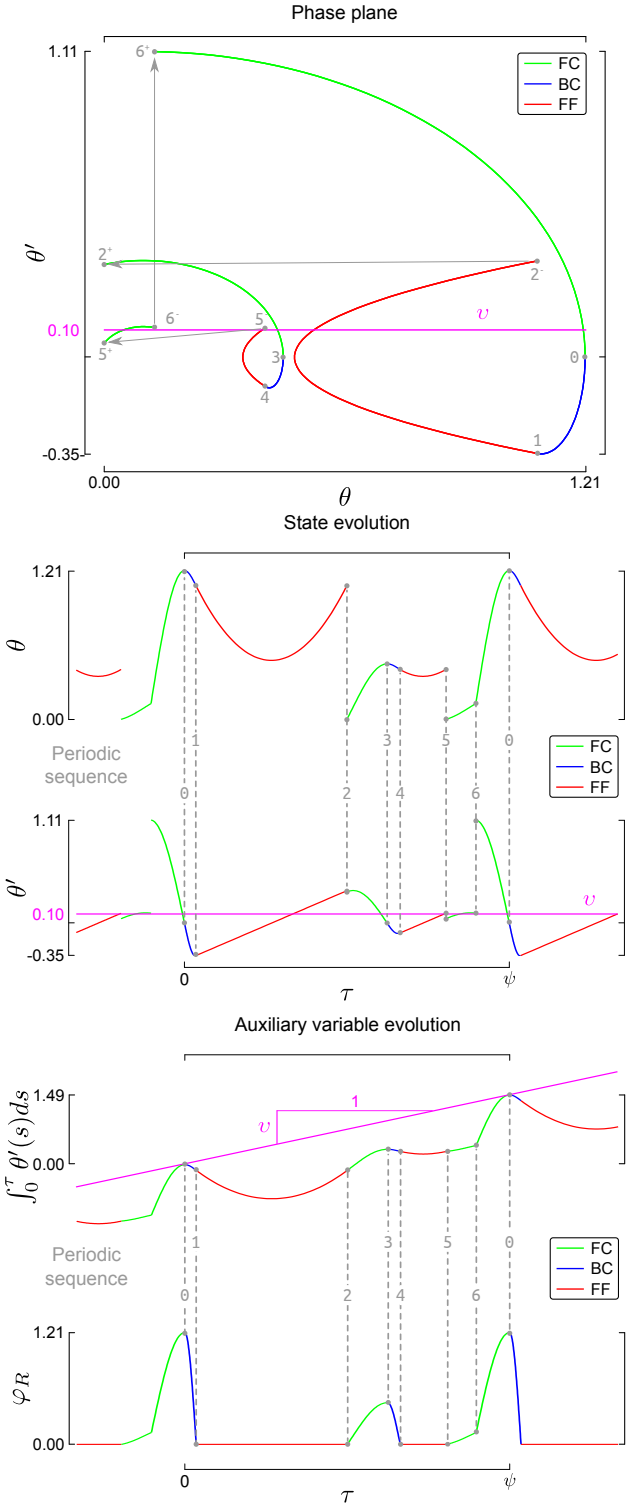

Figure 6: Example of period-1 ($n = 1$) limit cycle with two drilling cycles ($m = 2$), $(\gamma, \lambda_S, \psi, \kappa_0) = (10, 0.1, 15, 0.09)$ – Phase portrait and time evolutions of the (auxiliary) state variables. The periodic sequence is given by $((\mathsf{FC} \to \mathsf{BC} \to \mathsf{FF})_2 \to \mathsf{FC} \to \Delta\theta_i')_{\circlearrowleft}$.

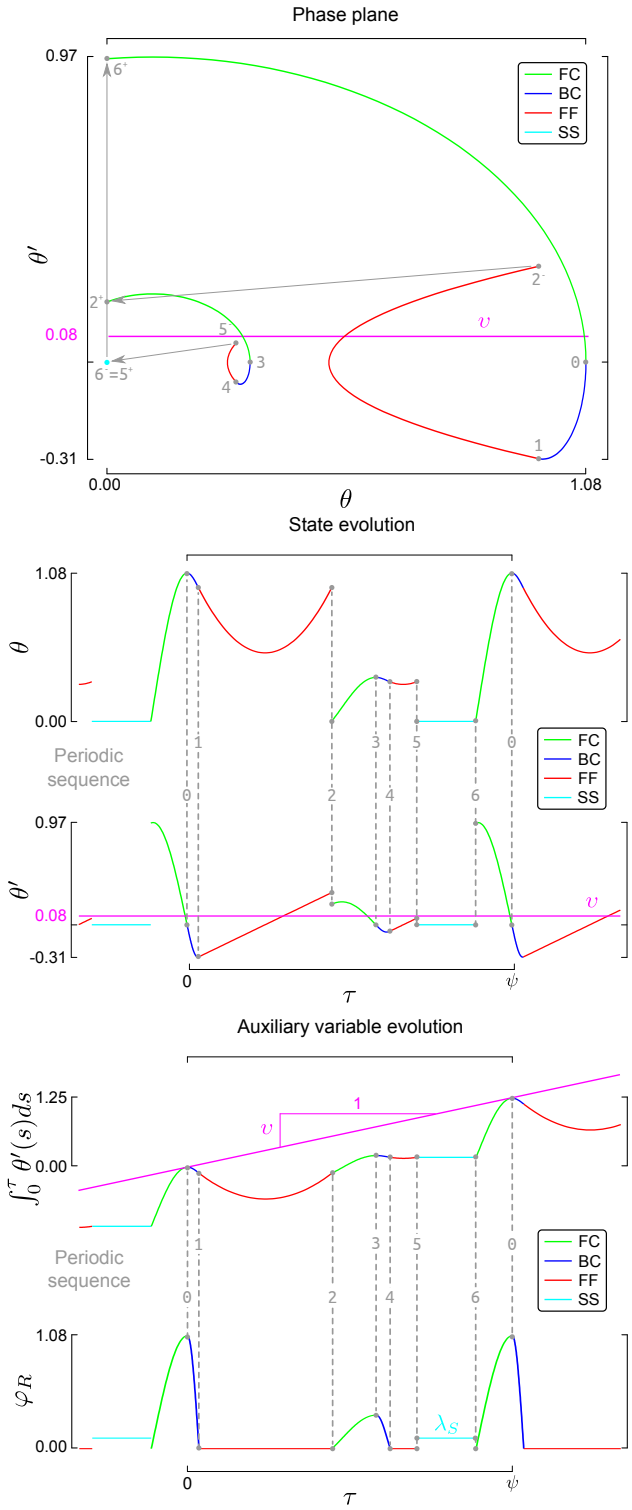

Figure 7: Example of period-1 ($n = 1$) limit cycle with two drilling cycles ($m = 2$), $(\gamma, \lambda_S, \psi, \kappa_0) = (10, 0.1, 15, 0.24)$ – Phase portrait and time evolutions of the (auxiliary) state variables. The periodic sequence is given by $((\mathsf{FC} \to \mathsf{BC} \to \mathsf{FF})_2 \to \mathsf{SS} \to \Delta\theta_i')_{\circlearrowleft}$. Once the bit enters the standstill phase, it remains at rest until the next activation.

examples illustrate typical periodic solutions of the model and show the influence of the energy barrier on the response of the system, with the larger value trimming the sequence of drilling cycles once the energy injected by the percussive activation has been dissipated by the penetration process. To facilitate the understanding of the responses depicted in Figures 6 and 7, the phase portraits are annotated following the sequence of drilling phases experienced by the system along the limit cycle and state discontinuities are indicated by arrows. State jumps correspond to either a reset of the penetration while drilling at the initiation of a new drilling cycle combined with a decrease of the bit velocity (oblique), a transition to standstill (oblique), or an impulsive activation (vertical). Complementary to the phase portraits, the time evolutions of the state variables (penetration while drilling θ and penetration rate θ') and those of the auxiliary variables (cumulative penetration $\int_0^\tau \theta'(s)ds$ and contact force φ_R) are also shown. Additionally, the average response is shown, underscoring the oscillatory motion of the bit around its average penetration during periodic or stationary drilling.

The first descriptor is inspired by the works on impact oscillators by Peterka et al. [42, 43], who have introduced the notion of average number of impacts to characterize the periodic response of these systems. We define the average number of drilling cycles per loading period as the ratio m/n between the number of drilling cycles m and the period multiplicity n, where we define a drilling cycle as a succession of forward and backward contact drilling phases. This measure provides a rough idea of the phase portrait topology while incorporating the period multiplicity at the same time. For both example limit cycles, the ratio is given by $m/n = 2/1$.

The second descriptor is richer but less readable. It corresponds to the explicit stipulation of the periodic sequence of drilling phases: $(\mathsf{BC} \to \mathsf{FF} \to \mathsf{FC} \to \mathsf{BC} \to \mathsf{FF} \to \mathsf{FC} \to \Delta\theta'_i \to \mathsf{FC})_{\circlearrowleft}$ and $(\mathsf{BC} \to \mathsf{FF} \to \mathsf{FC} \to \mathsf{BC} \to \mathsf{FF} \to \mathsf{SS} \to \Delta\theta'_i \to \mathsf{FC})_{\circlearrowleft}$, for examples one and two respectively. Accounting for the inner-periodicity of the sequence, they also synthetically read $((\mathsf{FC} \to \mathsf{BC} \to \mathsf{FF})_2 \to \mathsf{FC} \to \Delta\theta'_i)_{\circlearrowleft}$ and $((\mathsf{FC} \to \mathsf{BC} \to \mathsf{FF})_2 \to \mathsf{SS} \to \Delta\theta'_i)_{\circlearrowleft}$. Although not complete, this descriptor provides a fair inspiration as to the qualitative outline of the limit cycle phase portrait. It also enables recovery of the first one ($m/n = 2/1$), as two $\mathsf{FC} \to \mathsf{BC}$ transitions and one velocity jump appear in the periodic sequence.

The most complete descriptors are the phase portraits of the limit cycles themselves from which the previous descriptors are easily recovered. They contain all information about the limit cycles, but their time components. In particular, the projective nature of the phase portrait is visible in the degeneracy of the standstill phase into a single point, see Figure 7.

3.3. Preliminary analytical results

In dimensionless coordinates, the modified bilinear bit/rock interaction model depends on two parameters, namely $\gamma \in (1, \infty)$ and $0 \leq \kappa_0 < 1$. On the one hand, γ controls the dissipation associated with the bit/rock interaction on the timescale of bit motion, and we note that the interaction process degenerates into a conservative or a fully dissipative one as $\gamma \to 1$ and $\kappa_0 = 0$ or $\gamma \to \infty$, respectively. On the other hand, κ_0 represents the energy dissipation on the timescale of wave propagation in the rock medium and acts as an energy barrier to prevent indefinite penetration of the bit under a constant static load.

We now state some partial results from the analysis of the bit/rock interaction that illustrate the influence of both parameters and the expected behaviors of the system in specific conditions.

Consider the drilling cycle resulting from an initial velocity $\theta'_\ell \geq \kappa_0$ at the beginning of a forward contact phase in the absence of percussive activation, i.e. from initial conditions $(\theta_0, \theta'_0) = (0, \theta'_\ell)$. This corresponds to the sequence ABC depicted in the penetration/force (θ, φ_R)-plane of Figure 8. The energy consumed by the bit/rock inter-

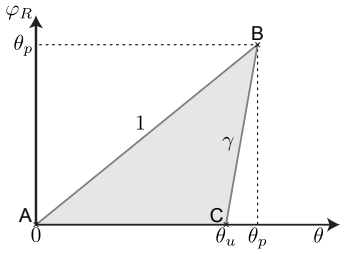

Figure 8: The energy dissipated by the bit penetration into the rock medium is given by the area delimited by the drilling cycle in the (θ, φ_R)-plane.

action process is given by the work done by the contact force plus the energy radiated in the rock medium $\kappa_0^2/2$. It is thus defined as the area of triangle ABC plus $\kappa_0^2/2$

$$\begin{aligned} W_{\varphi_R}^{\mathsf{ABC}} &= \int_0^{\theta_p} \varphi_R(s)ds + \int_{\theta_p}^{\theta_u} \varphi_R(s)ds + \frac{\kappa_0^2}{2}, \\ &= \frac{\theta_u \theta_p}{2} + \frac{\kappa_0^2}{2}. \end{aligned} \tag{16}$$

From the balance of energy along the drilling cycle and the transition conditions (14), the peak and upper penetrations can be related to the initial conditions

$$\theta_p = \lambda_S + \sqrt{\lambda_S^2 + \theta_\ell'^2 - \kappa_0^2}, \tag{17}$$

$$\theta_u = \frac{\gamma - 1}{\gamma}\left(\lambda_S + \sqrt{\lambda_S^2 + \theta_\ell'^2 - \kappa_0^2}\right), \tag{18}$$

and the rebound velocity is given by

$$\theta_u' = -\frac{1}{\sqrt{\gamma}}\sqrt{\theta_\ell'^2 - \kappa_0^2}. \tag{19}$$

These results are very instructive about the behavior of the system.

(i) In the absence of an energy barrier, $\kappa_0 = 0$, the system experiences unbounded penetration under the sole action of the vertical dead load. Indeed, considering the application of the static loading from rest conditions, $(\theta_\ell, \theta_\ell') = (0, 0)$, the state upon completion of the drilling cycle reads

$$(\theta_u, \theta_u') = (2\lambda_S, 0), \tag{20}$$

that is, the bit achieves non-zero penetration and exits the drilling cycle with zero velocity. Given the absence of an energy barrier, the system begins a new drilling cycle with zero velocity after the penetration and force on bit are reset to zero, i.e. it starts a new drilling cycle with initial conditions $(\theta_\ell, \theta_\ell') = (0, 0)$ identical to those of the original problem. The bit therefore achieves unbounded penetration under the static load through repetition of the drilling cycle. The energy barrier, in making a distinction between static and dynamic indentations, prevents such unphysical behaviors.

(ii) The energy consumed by the penetration process following a single percussive activation in the absence of dead load is given by

$$W_{\varphi_R}^{\mathsf{ABC}} = \frac{1}{2\gamma}\left(\gamma - 1 + \kappa_0^2\right). \tag{21}$$

A convenient parametrization of the energy barrier κ_0 is then

$$\kappa_0 = \epsilon\sqrt{\gamma - 1} \tag{22}$$

so that

$$W_{\varphi_R}^{\mathsf{ABC}} = \frac{\gamma - 1}{2\gamma}\left(1 + \epsilon^2\right). \tag{23}$$

(iii) Should the bit have a positive velocity $\theta_\ell' > \kappa_0$ at the beginning of a drilling cycle during which no percussive activation takes place, then it will necessarily exit the drilling cycle with a negative velocity and enter a free flight phase, leading to a sequence $(\mathsf{FC} \to \mathsf{BC} \to \mathsf{FF})$.

(iv) In the absence of percussive activation, the system entering the drilling cycle with initial conditions $(0, \theta_\ell')$ with $\theta_\ell' \geq \kappa_0$ experiences a succession of m sequences $(\mathsf{FC} \to \mathsf{BC} \to \mathsf{FF})$ until the energy barrier is reached, with

$$m = \left\lceil \frac{\ln\left(\theta_\ell'^2/\epsilon^2 + 1\right)}{\ln \gamma} \right\rceil - 1, \tag{24}$$

the brackets $\lceil \cdot \rceil$ denoting rounding operation to the nearest larger integer number. The m drilling cycles

complete after a duration

$$\psi_m = \sum_{i=1}^{m} \left\{ \left(1 + \frac{1}{\sqrt{\gamma}}\right) \left(\pi - \cdots \right. \right. \\ \left. \left. \cdots \operatorname{acos} \frac{\lambda_S}{\sqrt{\lambda_S^2 + \left(\theta'_{\ell,(i)}\right)^2}} \right) + \frac{2\theta'_{\ell,(i)}}{\sqrt{\gamma}\lambda_S} \right\}, \tag{25}$$

with

$$\theta'_{\ell,(i)} = \sqrt{\frac{\theta'^2_\ell}{\gamma^{i-1}} - \kappa_0^2 \frac{1-\gamma^{-i}}{1-\gamma^{-1}}}. \tag{26}$$

These two results follow from energy balance and the analytical solutions of the equations of motion.

(v) Setting $\theta'_\ell = 1$ in the above equations, namely post-activation conditions from standstill phase, provides a means to track period-1 solutions with a standstill phase. For a given set of parameters, m and ψ_m can be computed. The inequality $\psi \geq \psi_m$ then constitutes the existence condition of a limit cycle with periodic sequence $((\mathsf{FC}{\to}\mathsf{BC}{\to}\mathsf{FF})_m \to \mathsf{SS} \to \Delta\theta'_i)_{\circlearrowleft}$.

(vi) In the limit $\gamma \to 1$ and for $\kappa_0 = 0$, the rebound velocity has the same magnitude as the initial velocity but with opposite sign. This is the translation of the conservative nature of the degenerated bit/rock interaction, for it degenerates into a linear spring in unilateral contact with the bit. In the limit $\gamma \to 1$ and for $\kappa_0 > 0$, the energy barrier will dissipate energy at each closure of the contact interface and the rebound velocity is lower than the impact one, ultimately leading to a state of rest. In either case, no penetration is achieved on average.

(vii) In the limit $\gamma \to \infty$, the rebound velocity vanishes whatever the magnitude of the initial velocity. This corresponds to a fully dissipative interaction law, i.e. $(\theta_u, \theta'_u) = (\theta_p, 0)$. System motion is then given by $(\mathsf{FC} \to \mathsf{SS} \to \Delta\theta'_i)_{\circlearrowleft}$ provided $\psi \geq \pi$ and the average rate of penetration reads

$$\upsilon = \frac{\lambda_S + \sqrt{\lambda_S^2 + 1 - \kappa_0^2}}{\psi}. \tag{27}$$

Backward contact and free flight phases become inaccessible.

(viii) The standstill phase is an absorbant mode for the dynamical system. Two consequences follow:

(a) Any trajectory that enters a standstill phase is stuck in this phase until the next activation. As such, the standstill phase acts as a reset of the system initial conditions to $(\theta_\ell, \theta'_\ell) = (0, 1)$ at the time of next activation.

(b) The zero vector field associated with the standstill phase leads to a zero fundamental solution matrix during that arch of trajectory. Accordingly, limit cycles containing a standstill phase are super-stable in the sense that both Floquet multipliers are zero, i.e. the trajectory exactly returns on the limit cycle after one period provided perturbations do not preclude the presence of the standstill phase in the perturbed motion sequence.

3.4. Parametric analysis

To evaluate the influence of the feed force on the steady-state response of the system, we have subjected the solution of the governing equations to the continuation procedure described in Section 3.1, for parameters $(\gamma, \psi, \kappa_0) = (10, 10, 0.09)$. The bifurcation diagram of Figure 9 is the result of this investigation. The upper plot shows the average penetration rate, as computed from the steady-state limit cycle, while the lower one represents the number m of drilling cycles the periodic response comprises. Superposed is a color code relative to the stability of the periodic response: blue markers denote asymptotically stable solutions while red ones pertain to unstable responses. The bottom plot is also annotated with the average number of drilling cycles, for this is the simplest and most legible descriptor of the phase portrait outline.

Analysis of the plots of Figure 9 leads to the following observations.

(i) The model response shows clues of the experimentally-observed optimal configuration reproduced in Fig-

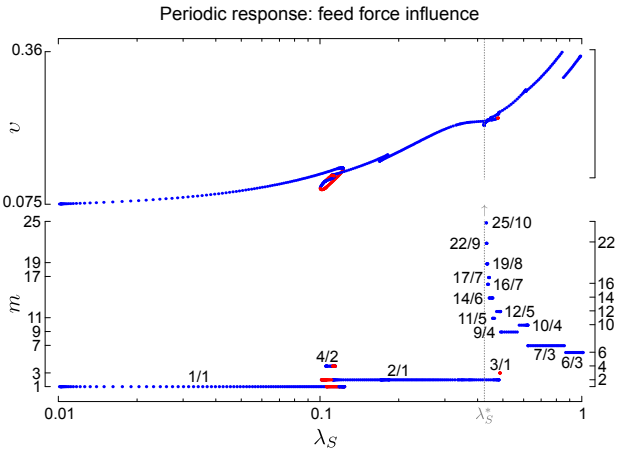

Figure 9: Periodic response, $(\gamma, \psi, \kappa_0) = (10, 10, 0.09)$. Unstable (red markers) and stable (blue markers) configurations.

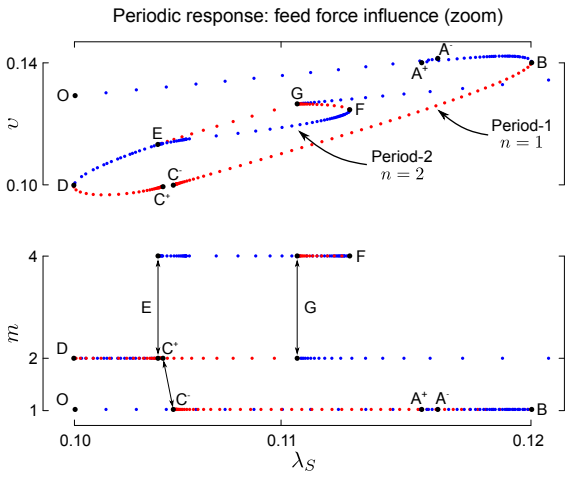

Figure 10: Periodic response, $(\gamma, \psi, \kappa_0) = (10, 10, 0.09)$, $\lambda_S \in [0.10, 0.12]$ range. Unstable (red markers) and stable (blue markers) configurations.

ure 5. There exists local maxima of the average penetration rate with respect to the vertical load in the simulated response. To the knowledge of the authors, the physical cause of the optimum experienced in field conditions is unknown. These results plead, however, in favor of the optimum being the consequence of the process dynamics rather than being due to an intrinsic change of the nature of the bit/rock interaction such as the ductile to brittle failure transition that can be observed in conventional rotary drilling [23, 44].

(ii) In range $\lambda_S \in [0.10, 0.12]$, multiple periodic responses do exist. Figure 10 proposes an enlargement of this area, where the coexisting solutions may differ by their average number of drilling cycles or their stability. This enlargement also shows the discontinuous characteristic certain bifurcations present. This feature is to be related to the non-commutativity of the percussive activation and the instantaneous dissipation associated with the energy barrier. See Appendix for more details.

Following the period-1 response from its leftmost point, point O, we see that the solution undergoes bifurcations of different kinds. At point A, the bifurcation diagram is discontinuous. It corresponds to the transition between periodic sequence (FC $\rightarrow$ BC $\rightarrow$ FF $\rightarrow \Delta\theta_i' \rightarrow$ FF)$_{\circlearrowleft}$ (A^-) and (FC $\rightarrow$ BC $\rightarrow$ FF $\rightarrow$ FC $\rightarrow \Delta\theta_i'$)$_{\circlearrowleft}$ (A^+), when activation takes place at the moment the bit contacts the rock at the transition FF $\rightarrow$ FC. Point B corresponds to a loss of stability of the 1/1 limit cycle through a fold bifurcation. Another discontinuity occurs at point C with the apparition of a second drilling cycle within the periodic solution. This unstable 2/1 limit cycle then regains stability at point D via a second fold bifurcation and loses it again at point E, consequently to a flip bifurcation. Point E thus also corresponds to the origin of a branch of period-2 orbits. They have an average number of drilling cycles 4/2, are stable on branch EF and unstable along FG. A fold bifurcation at point F is responsible for the change of stability. The 2/1 solution is again stable from point G on to larger values of the dead load λ_S. Jumps from one attractor to another may thus be expected in this region, were the system subjected to external perturbations, likely engendering complex dynamics.

(iii) A major bifurcation occurs at $\lambda_S = \lambda_S^* = 0.43$, for the response of the system dramatically changes once the vertical dead load is increased past that value.

This bifurcation corresponds to the appearance of a standstill phase in the periodic sequence. Confirmation of this abrupt change of behavior is given by the stroboscopic Poincaré map of the system (Figure 11) that depicts the state of the system prior to impact. On the map is also visible the change of periodicity of the limit cycle as λ_S varies.

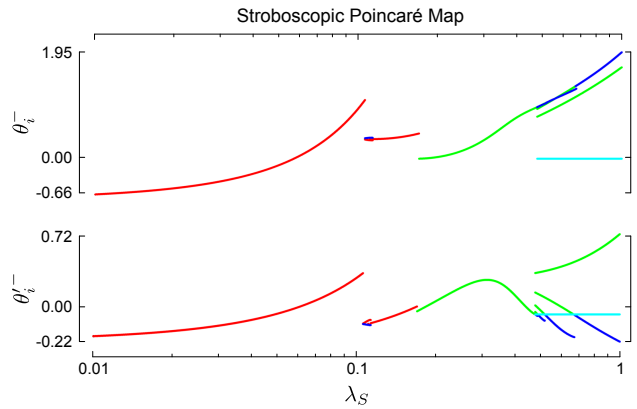

Figure 11: Stroboscopic Poincaré map at $\tau = \tau_i^-$, $(\gamma, \psi, \kappa_0) = (10, 10, 0.09)$. The map displays 500 points that were sampled after removal of a transient of 500 periods. The system was initialized in standstill phase.

At the bifurcation point, the number of drilling cycles increases dramatically. Numerics nonetheless show that this increase verifies a bounded average number of drilling cycles as it remains in the range $[2, 3]$ observed on the nearby branches corresponding to periodic solutions without standstill. Past the bifurcation, for $\lambda_S \in [\lambda_S^*, 1]$, discontinuities of the average rate of penetration follow from changes in the periodic sequence.

4. Conclusion

In this paper, we have presented a low dimension model for the study of the process of percussive drilling. This novel model combines elements previously studied in the literature but that, to the knowledge of the authors, had not been assembled before: a drifting oscillator impulsively loaded coupled with a bilinear bit/rock interaction law, together with an energy barrier. The assembly of these building blocks has resulted in a hybrid dynamical system governed by four drilling phases and associated mode transition conditions.

A preliminary analysis of the model has shown the necessity of complementing the bilinear force/penetration law by an energy barrier to differentiate the cases of static and dynamic indentations and prevent unbounded penetration under static loading. Consequent to the energy barrier is an instantaneous dissipation of kinetic energy at the moment the bit contacts the rock. This analysis has also shed light on some expected behaviors of the system. In particular, the standstill phase has been shown to be an absorbant element of the dynamical system, acting as a reset of the initial conditions.

Results of numerical simulations by use of techniques tailored to hybrid systems have revealed three main facts. First, the model appears to recover an experimentally-observed trend; that is, the existence of local maxima of the average steady-state penetration rate with respect to the vertical load on bit. Second, for given ranges of the vertical load, the studied configurations exhibit coexistence of stable and unstable limit cycles. Complex responses are likely to be observed in these regions. Third, at larger loads, periodic solutions comprise a standstill phase; that is, the bit performs a certain number of drilling cycles under the percussive activation before coming to rest until the next activation takes place.

Similarly to the results obtained by Ajibose et al. [29], our analysis also shows evidence of the existence of an optimum drilling configuration. There are, however, fundamental differences between the two drifting oscillator models of the drilling process. First, our model relies on an impulsive activation while theirs is based on a harmonic one; second, the bilinear interface law we propose incorporates an energy barrier, while the polynomial laws they use do not. These choices limit the applicability of the models to certain parameter ranges, ranges that may be related to

the technology the model is associated with. In particular, our model attempts at representing percussive drilling (impulsive activation at frequencies $\mathcal{O}(10)$ Hz) whereas theirs is aimed at describing ultrasonic drilling and machining (high frequency harmonic activation at a frequencies $\mathcal{O}(1)$ kHz).

Further investigations are required to deeper understand the dynamics of the process described by the proposed model, in addition to the comprehension of the bifurcations taking place in the system when parameters are swept. More specifically, we expect the understanding of the dynamics to lead to the identification of the conditions related to optimal drilling.

Acknowledgments

This research was supported by the Commonwealth Scientific and Industrial Research Organisation (CSIRO) and by Itasca International Inc. These supports are gratefully acknowledged.

References

[1] P.A. Bartelt, W. Ammann, and E. Anderheggen. The numerical simulation of the impact phenomena in nail penetration. *Nucl. Eng. Des.*, 150:431–440, 1994.

[2] P. Villaggio. Hammering of Nails and Pitons. *Math. Mech. Solids*, 10(4):461–468, August 2005.

[3] P. Kettil, G. Engstrom, and N. Wiberg. Coupled simulation of wave propagation and water pumping phenomenon in driven concrete piles. *Comput. Struct.*, 85(3-4):170–178, February 2007.

[4] U.V. Lê. A general mathematical model for the collision between a free-fall hammer of a pile-driver and an elastic pile: Continuous dependence and low-frequency asymptotic expansion. *Nonlinear Anal.-Real.*, 12(1):702–722, February 2011.

[5] L. Zhou, J. Chen, and W. Lao. Construction Control and Pile Body Tensile Stresses Distribution Pattern during Driving. *J. Geotech. Geoenviron.*, 133(9):1102–1109, 2007.

[6] G.L. Cavanough, M. Kochanek, J.B. Cunningham, and I.D. Gipps. A Self-Optimizing Control System for Hard Rock Percussive Drilling. *IEEE-ASME T. Mech.*, 13(2):153–157, April 2008.

[7] L.E. Chiang and D.A. Elias. Modeling impact in down-the-hole rock drilling. *Int. J. Rock Mech. Min.*, 37(4):599–613, June 2000.

[8] E. Nordlund. The Effect of Thrust on the Performance of Percussive Rock Drills. *Int. J. of Rock Mech. Min. Sci. Geomech. Abstr.*, 26(I):51–59, 1989.

[9] W.A. Hustrulid and C.E. Fairhurst. Theoretical and Experimental Study of Percussive Drilling of Rock - Part I - Theory of Percussive Drilling. *Int. J. Rock Mech. Min.*, 8(4):311–333, July 1971.

[10] B.R. Stephenson. *Measurement of Dynamic Force-Penetration Characteristics in Indiana Limestone.* Master's thesis, University of Minnesota, 1963.

[11] B. Haimson. *High Velocity, Low Velocity and Static Penetration Characteristics in Tennessee Marble.* Master's thesis, University of Minnesota, 1965.

[12] W.A. Hustrulid and C.E. Fairhurst. Theoretical and Experimental Study of Percussive Drilling of Rock - Part II - Force-Penetration and Specific Energy Determinations. *Int. J. Rock Mech. Min.*, 8(4):335–356, July 1971. doi: 10.1016/0148-9062(71)90046-5.

[13] L.G. Karlsson, B. Lundberg, and K.G. Sundin. Experimental study of a percussive process for rock fragmentation. *Int. J. Rock Mech. Min. Sci. Geomech. Abstr.*, 26(1):45–50, January 1989.

[14] S. Y. Wang, S. W. Sloan, H. Y. Liu, and C. A. Tang. Numerical simulation of the rock fragmentation process induced by two drill bits subjected to static and dynamic (impact) loading. *Rock Mech. Rock Eng.*, 44(3):317–332, November 2010.

[15] T. Saksala. Numerical modelling of bit–rock fracture mechanisms in percussive drilling with a continuum approach. *Int. J. Numer. Anal. Meth. Geomech.*, 35:1483–1505, 2011.

[16] F. Zhang and H. Huang. Discrete Element Modeling of Sphere Indentation in Rocks. In *45th US Rock Mechanics / Geomechanics Symposium*, San Francisco, CA, U.S.A., 2011. American Rock Mechanics Association.

[17] X. Li, G. Rupert, and D.A. Summers. Energy transmission of down-hole hammer tool and its conditionality. *T. Nonferr. Metal Soc.*, 10(1):109–113, 2000.

[18] B. Lundberg. Microcomputer simulation of percussive drilling. *Int. J. Rock Mech. Min. Sci.*, 22(4):237–249, August 1985.

[19] A.M. Krivtsov and M. Wiercigroch. Dry friction model of percussive drilling. *Meccanica*, 34(6):425–435, December 1999.

[20] A.M. Krivtsov and M. Wiercigroch. Penetration rate prediction for percussive drilling via dry friction model. *Chaos Soliton. Fract.*, 11(15):2479–2485, December 2000.

[21] E. Pavlovskaia, M. Wiercigroch, and C. Grebogi. Modeling of an impact system with a drift. *Phys. Rev. E*, 64:56224–56229,

November 2001.

[22] H. Alehossein, E. Detournay, and H. Huang. An Analytical Model for the Indentation of Rocks by Blunt Tools. *Rock Mech. and Rock Eng.*, 33(4):267–284, 2000.

[23] H. Huang and E. Detournay. Intrinsic Length Scales in Tool-Rock Interaction. *Int. J. Geomech.*, 8(1):39–44, 2008.

[24] O.K. Ajibose. *Nonlinear Dynamics and Contact Fracture Mechanics of High Frequency Percussive Drilling*. Ph.D. thesis, University of Aberdeen, 2009.

[25] W. Changming. An analytical study of percussive energy transfer in hydraulic rock drills. *Min. Sci. Technol.*, 13(1):57–68, July 1991.

[26] M. Amjad. *Control of ITH Percussive Longhole Driling in Hard Rock*. Ph.D. thesis, McGill University, Montreal, Quebec, Canada, 1996.

[27] G. Pearse. Hydraulic rock drills. *Min. Mag.*, pages 220–231, March 1985.

[28] O.K. Ajibose, M. Wiercigroch, E. Pavlovskaia, and A.R. Akisanya. Contact force models and the dynamics of drifting impact oscillator. In V Denoel and E Detournay, editors, *First International Colloquium on Non-Linear Dynamics of Deep Drilling Systems*, pages 33–38, 2009.

[29] O. K. Ajibose, M. Wiercigroch, E. Pavlovskaia, A. R. Akisanya, and G Károlyi. Drifting Impact Oscillator With a New Model of the Progression Phase. *J. Appl. Mech.*, 79(6):061007–1–9, November 2012.

[30] M. di Bernardo, C.J. Budd, A.R. Champneys, and P. Kowalczyk. *Piecewise-smooth Dynamical Systems - Theory and Applications*, volume 163. Springer-Verlag London Ltd., 2008.

[31] R.I. Leine and H. Nijmeijer. *Dynamics and Bifurcations of Non-Smooth Mechanical Systems*. Springer-Verlag Berlin Heidelberg, 2004.

[32] R.I. Leine. Bifurcations of equilibria in non-smooth continuous systems. *Physica D*, 223(1):121–137, November 2006.

[33] G. Luo and J. Xie. Bifurcations and chaos in a system with impacts. *Physica D*, 148(3-4):183–200, January 2001.

[34] J.J.P. Veermana, D. Daescua, M.J. Romero-Vallésb, and P.J. Torres. A single particle impact model for motion in avalanches. *Physica D*, 238(19):1897–1908, 2009.

[35] B. Lundberg and M. Okrouhlik. Efficiency of a percussive rock drilling process with consideration of wave energy radiation into the rock. *International Journal of Impact Engineering*, 32: 1573–1583, 2006.

[36] V. Acary and B. Brogliato. *Numerical Methods for Nonsmooth Dynamical Systems. Applications in Mechanics and Electronics*. Springer Verlag Berlin Heidelberg, 2008.

[37] A.H. Nayfeh and B. Balachandran. *Applied Nonlinear Dynamics: Analytical, Computational and Experimental Methods*. Wiley-VCH Verlag GmbH and Co. KGaA, Weinheim, 1995.

[38] R. Seydel. *Practical bifurcation and stability analysis*. Springer New York Dordrecht Heidelberg London, 2009.

[39] A.M.P. Valli, R.N. Elias, G.F. Carey, and A.L.G.A. Coutinho. PID adaptive control of incremental and arclength continuation in nonlinear applications. *Int. J. Numer. Meth. Fl.*, 61:1181–1200, 2009.

[40] J. Awrejcewicz and C.-H. Lamarque. *Bifurcation And Chaos In Nonsmooth Mechanical Systems*. World Scientific Publishing Co., 2003.

[41] A. Depouhon, E. Detournay, and V. Denoël. Limit Cycling Behavior of a Hybrid System: Application to Percussive Drilling. In N. van de Wouw and E. Detournay, editors, *Second International Colloquium on Non-Linear Dynamics and Control of Deep Drilling Systems*, pages 77–86, 2012.

[42] F. Peterka and J. Vacik. Transition to chaotic motion in mechanical systems with impacts. *Journal of Sound and Vibration*, 154(1):95–115, 1992.

[43] F. Peterka. Dynamics of Double Impact Oscillators. *Facta Univ. Ser. Mech. Automat. Control Robot.*, 2(10):1177–1190, 2000.

[44] T. Richard. Determination of rock strength from cutting tests. M.S. thesis, University of Minnesota, 1999.

A. Non-commutativity of the percussive activation and energy barrier

To illustrate the reason underlying the discontinuities of the bifurcation diagram along the branches corresponding to periodic orbits without standstill phase, we consider the one occurring at point A of Figure 9. Left of it ($\lambda_S < \lambda_S|_{A^-}$, branch OA^-), the periodic sequence is given by $(\mathsf{FC} \to \mathsf{BC} \to \mathsf{FF} \to \Delta\theta'_i \to \mathsf{FF})_{\circlearrowleft}$. Right of it ($\lambda_S > \lambda_S|_{A^+}$, branch $\mathrm{A}^+\mathrm{B}$), it is $(\mathsf{FC} \to \mathsf{BC} \to \mathsf{FF} \to \mathsf{FC} \to \Delta\theta'_i)_{\circlearrowleft}$. Thus, the limiting case corresponds to the periodic sequence $(\mathsf{FC} \to \mathsf{BC} \to \mathsf{FF} \to \Delta\theta'_i)_{\circlearrowleft}$ and must be considered for a vanishing FF (A^-) or FC (A^+) phase.

Starting with the A^- case, we write the periodicity conditions of the orbit by following its periodic sequence, from initial conditions $(0, \theta'_\ell)$ in FC phase, i.e. before the energy barrier is applied. It reads

$$\theta'_\ell = \sqrt{\frac{\theta'^2_\ell - \kappa_0^2}{\gamma}} + 1, \tag{28}$$

and

$$\psi = \left(1+\frac{1}{\sqrt{\gamma}}\right)\left(\pi-\operatorname{acos}\frac{\lambda_S}{\sqrt{\lambda_S^2+\theta_\ell'^2-\kappa_0^2}}\right)\cdots + \cdots+\frac{2}{\lambda_S}\sqrt{\frac{\theta_\ell'^2-\kappa_0^2}{\gamma}}. \quad (29)$$

While the former equation has a closed-form solution

$$\theta_\ell' = \frac{\sqrt{\gamma}}{\gamma-1}\left(\sqrt{\gamma}+\sqrt{1-\frac{\gamma-1}{\gamma}\kappa_0^2}\right), \quad (30)$$

the latter requires a numerical resolution. Considering the numerical parameters of the bifurcation analysis, namely $(\gamma,\psi,\kappa_0)=(10,10,0.09)$, we find

$$(\lambda_S,\theta_\ell') = (0.1178, 1.4610). \quad (31)$$

Then we write the periodicity conditions assuming the activation no longer takes place during the FF phase but during the FC one. They read

$$\theta_\ell' = \frac{1}{\sqrt{\gamma}}\left(\sqrt{\theta_\ell'^2-\kappa_0^2}+1\right), \quad (32)$$

$$\psi = \left(1+\frac{1}{\sqrt{\gamma}}\right)\left(\pi-\operatorname{acos}\frac{\lambda_S}{\sqrt{\lambda_S^2+\left(\sqrt{\theta_\ell'^2-\kappa_0^2}+1\right)^2}}\right) + \frac{2}{\lambda_S}\frac{\sqrt{\theta_\ell'^2-\kappa_0^2}+1}{\sqrt{\gamma}}. \quad (33)$$

Again, the first condition can be solved analytically for the velocity

$$\theta_\ell' = \frac{1}{\gamma-1}\left(\sqrt{\gamma}+\sqrt{1-(\gamma-1)\kappa_0^2}\right) \quad (34)$$

but the second requires a numerical procedure to be solved for λ_S. Using the numerical parameters of the bifurcation analysis, we obtain

$$(\lambda_S,\theta_\ell') = (0.1170, 0.4579) \quad (35)$$

which is different from result (31). The limiting behaviors from the left and from the right are thus different, and this difference stems from the non-commutativity of the percussive activation and the energy barrier with respect to periodic responses of the system.

Discontinuities of the bifurcation diagram are therefore expected whenever the activation passes from a FF phase to a FC one, and when a new drilling cycle appears in the periodic sequence, through a BC $\rightarrow \Delta\theta_i \rightarrow$ FC transition. Should $\kappa_0 = 0$, the bifurcation diagram of Figure 10 would then be continuous at points A and C.